Cruz-Peragón, F., Gómez-de la Cruz, F. J., Palomar-Carnicero, J. M., & López-García, R. (2022). Optimal design of a hybrid ground source heat pump for an official building with thermal load imbalance and limited space for the ground heat exchanger. *Renewable Energy*, *195*, 381-394.

https://doi.org/10.1016/j.renene.2022.06.052

Optimal design of a hybrid Ground Source Heat Pump for an official building with thermal load imbalance and limited space for the Ground Heat Exchanger.

Authors.

Cruz-Peragón, F.[1], Gómez-de la Cruz F.J.[1*], Palomar-Carnicero J.M. [1], López-García R[1].

[1]Dep. of Mechanical and Mining Engineering, Escuela Politécnica Superior de Jaén, University of Jaén, Campus Las Lagunillas s/n, 23071, Jaén (Spain).

Abstract.

This work presents the optimal design of a hybrid ground source heat pump (GSHP), taking into account thermal imbalance and space limitation for the ground heat exchanger field (GHE), applied to an official building. Once the building loads are calculated and devices selected, experiments carried out from a single vertical borehole obtain the ground thermal characteristics, including a local short-term period function (STGF). From them, the Finite Line-Source (FLS) model simulates the GHE behavior, from decomposing the ground thermal loads in hourly linear steps for 50 years. A set of input variables, such as geometric configuration data of boreholes field, and additional terms associated with this hybrid operation, must be provided to the model. For optimization purposes, a design of experiments (DoE) considers the thermal ground characteristics and input factors, providing both energy savings and the internal rate of return as outputs (objective functions). Pareto's optimal solutions method provides the selected case, considering a compromise between economic and environmental benefits. It has been established for 18 boreholes (rectangular disposition) of 120 meters deep,

providing a 33.12% energy saving and an internal rate of return of 3.9%, also showing 89% of the total building load supported by the GHE.

KEYWORDS: GSHP system; G-function; FSL model; Geothermal Heat exchanger; Building Energy Efficiency; Pareto.

ABBREVIATIONS.

ANN	Artificial Neural Network
DoE	Design of Experiments
EW	Equal Weighted
FFDoE	Full Factorial Design of Experiments
FLS	Finite Line Source Model
GA	Genetic Algorithm
GHE	Ground Heat Exchanger
GSHP	Ground Source Heat Pump
GHG	Greenhouse Gasses Emissions
GTT	Ground Temperature Test
HP	Heat Pump
HVAC	Heating-Ventilation-Air Conditioning
IF	Input Factors
ILS	Infinite Line Source Model
LCA	Life Cycle Analysis
LGE	Lower Greenhouse Gas Emission
LTGF	Long-term g-function

REE	Red Eléctrica de España
RSM	Response Surface Methodology
STGF	Short-term g-function
TRT	Thermal Response Test

NOMENCLATURE

Latin letters

a	Constant (ºC) of aggregated term in ILS equation depending on ln(τ)
c	Cost (€/kWhe)
C	Volumetric Heat Capacity ($J \cdot m^{-3} \cdot K^{-1}$)
COP	Coefficient of Performance
e	Discount Rate
EER	Energy Efficiency Ratio
ES	Energy Savings (%)
eS	Energy Savings (MWh/year)
f	Approach Function of COP and EER
g	g-function
H	Depth (m)
i	Current hour
I	Investment cost (€)
IRR	Internal Rate of Return (%)
j	Current year
L	Length (m)
m	Slope ($°C \cdot s^{-1}$) in ILS equation depending on ln(τ)

N	Number of elements or Piles
NPC	Net Present Cost (€)
NPV	Net Present Value (€)
PB	Payback Period (year)
q	Unitary Heat pulse ($W \cdot m^{-1}$)
Q	Thermal load (kW)
r	Radius (m)
r/q	Rectangular/quincunx shape
R	Thermal Resistance ($m \cdot K \cdot W^{-1}$)
Re	Reynolds (dimensionless)
SF	Shave factor (%)
SPB	Simple Payback Period (year)
T	Temperature (ºC, K)
W	Electrical work of the compressor in the HP (MWh/y)

Greek Letters

α	Thermal Diffusivity ($m^2 \cdot s^{-1}$)
γ	Euler's Constant (dimensionless)
Δce	Annual Increment of electricity price (dimensionless)
λ	Thermal Conductivity ($W \cdot m^{-1} \cdot K^{-1}$)
τ	Time (s, h)
ϕ	Diameter (m)

Subscripts

av	Average
aux	Auxiliary
b	Borehole
B	Building
c	Compressor
cond	Condenser
dim	Dimensional
e	Electric
ev	Evaporator
ext	External
f	Fluid
H	Heating
i	Number of hour
int	Internal
L	Lower
max	Maximum
R	Refrigeration
reg	Regeneration
s	Soil
U	Upper
0	Experiment

1. Introduction.

Andalusia is the warmest region of Spain, where temperatures can reach more than 45ºC in summer, while several zones drop their temperatures below zero degrees in winter [1]. On the one hand, it justifies the use of efficient HVAC systems to reach adequate ambient conditions in buildings. On the other hand, the environment in this particular region causes thermal load imbalances making the HVAC systems reject more heat towards ambient in summer than the corresponding captured one in summer by the heat pumps (cooling-dominated). In any case, the buildings' energy consumption (electricity) to cover their loads for adequate heating and cooling constitutes a significant source of primary mover consumption and emissions. Therefore, apart from the main improvements that can be adopted to reduce them, both passive and active, a promoting alternative such as the GSHP can contribute significantly to these reductions, leading to CO_2 saving emissions [2]. Passive improvements consist of the envelope isolation and the internal shape or orientation of the building. On the other hand, active improvements are based on increasing the components' efficiency of the HVAC system, such as compressor, heat exchangers, thermodynamic cycle, or device control. This kind of HVAC system has been adopted worldwide, increasing significantly during the last years, exceeding 77,000MWt installed until 2020 [3]. In Spain, the share of energy from renewable sources in HVAC systems (including geothermal) was increased from 9.6% in 2004 to 16.9% in 2019 [4], which was used to produce 3,542TJ/y the current year [5]. It maintains a growing trend, helping to reach, next to other solutions, the objectives of overall decarbonisation in the near future. Particularly, this region has adopted vertical boreholes, which need smaller areas and present higher efficiencies [6]. In any case, the first stage to convince potential customers to install a GHSP system into a building consists of designing it conveniently, demonstrating the energy/environmental and economic costs savings in front of a conventional HVAC system.

Design methods of Ground Source Heat Pump (GSHP) systems with vertical boreholes involve evaluating the total length, L_{GHE} (m), of the Ground Heat Exchanger (GHE) field, which are capable of using as efficient as possible the HP for heating and cooling loads. For this purpose, the most advanced procedures vary the total length of a particular field configuration, evaluating the ground response temperature along time by an energy balance at each step. The iterative process finishes when the carrier fluid temperature does not exceed the imposed limits in the GHE (0ºC in winter and 35ºC in summer) throughout all the time evaluated (25 years). A deep description of the existing models and sizing tools can be reviewed in these references [7, 8]. Concerning most used models, both based on analytical infinite line source (ILS) and analytical finite line source (FLS) methods are applied to single-pile for ground characterization purposes from thermal response test (TRT) results. Other ones, such as finite difference and finite element/volume models, can be quite accurate for a complete GHE simulation, so sizing tools based on them provide quite reliable results due to their accuracy. Nevertheless, each simulation requires long computation times, involving an extremely computational charge because of a multi-objective optimization process to provide an optimal sizing. Therefore, they are impractical for design applications into a prudential period, but are recommended for customized detailed plant modelling by experimented users. Finally, the so-called analytical response factor models extend the use of the FLS method, applying a response factor of the ground attached to the GHE. The major of the analytical sizing tools are based on this last method (such as ASRHAE or EED), adapting to a friendly environment for designers. They can be associated with different categories related to the detail level of the model applied, being tighter as the sample time is shorter, up to hourly evaluation.

In this model, thermal ground characteristics are included, as well as a temperature response factor, called g-function [9, 10]. This function depends on time, borehole geometry, and ground characteristics and can be properly constructed for a complete GHE field (formed by several holes) by superimposing in space this initial function for a single borehole [11]. This g-function is composed of a short-term period function (STGF) and a long-term one (LTGF). Although, in the beginning, the last term (LTGF) was numerically estimated, it was validated later in an analytical and useful way [12]. In relation to the STGF, there are several methods to approximate it, such as numerically [13] and even by Artificial Neural Networks (ANN) [14]. In any case, they are generated synthetically, implying minor mismatches with a lack of accuracy when the response factor model is run with very short time steps [7]. In this sense, an experimental technique has been recently validated to provide this STGF, with the advantage of being evaluated for the own location where the GHE will be drilled [15]. Therefore, data from an initial test can provide it with excellent accuracy, overcoming the previous disadvantage.

However, selecting an adequate L_{GHE} does not suppose itself to be an optimal design. The economy plays a fundamental role in adopting these types of systems due mainly to their installation costs [16]. In addition, the degradation of the ground thermal condition over time causes a reduction of the GSHP efficiency [17], making the associated reduction of operating costs to be less than those activities expected. The Net Present Cost method (NPC) is selected as the principal economic indicator for this purpose [16]. In this sense, hybrid systems have been suggested to provide the major building thermal load from the GHE, while peak loads are supported by the conventional way. Therefore, the GSHP efficiency losses are minimized over time, overcoming the overall lifetime cost limiting factor [18, 19]. Several control strategies

200 are used for balancing the cooling and heating loads, such as limiting the fluid
201 temperature (set point control) or regenerating the soil (injecting or extracting heat flow
202 throughout the GHE) [18, 20]. In any case, a minimum lifetime system cost does not
203 suppose the best environmental solution, related to greenhouse emissions (GHG) and
204 others, as well as the primary mover. In fact, they are usually contradictory. This
205 environmental point of view has been commonly evaluated from the Life Cycle
206 Analysis of the installation (LCA) [21]. It considers all the steps associated with the HP,
207 from raw materials to the final disposal of equipment, obviously going through the
208 repercussion of its operation during its useful life (mainly by electricity use). The
209 lifetime GHG emissions (LGE) can be used as an indicator of this task [16].
210 Furthermore, several impacts can be evaluated, such as resource depletion, human
211 health, or ecosystem quality.
212 Both tasks, economic and environmental, can be evaluated by considering
213 savings instead of the overall lifetime study separately for conventional and with GHE
214 uses:
215 i) All environmental charges associated with the equipment (raw material,
216 production, transportation, final disposal, etc.) are the same, independently of the use of
217 the HP device. There is only one difference associated with the borehole setting-up by
218 drilling, inserting pipes and backfilling the grouts. Nevertheless, its influence is
219 relatively low for long lifetime use of the GHE (for instance, below 2% for GHG, below
220 1% for human toxicity, or around 3% for fossil depletion), pointing that removing it
221 from the overall environmental analysis does not imply substantial errors [21]. As the
222 main factor corresponds to the electricity (the largest contributor to the environmental
223 charges in an HP), the energy savings (ES) at operating conditions constitute a key
224 indicator of the differential environmental charge among conventional and GHE use of

the HP. From an energy/environmental point of view, this value should be above 25%, considering the efficiency improvements due to the GSHP use in a building with a balanced thermal load [22].

ii) In addition, the economic factors can be estimated between both HP uses for a known electricity cost. Therefore, an economic assessment can be applied to the GHE investment costs instead of the NPC for the overall lifetime separately. In this sense, investment selection criteria such as the net present value (NPV) or internal rate of return (IRR) are useful indicators to be evaluated [23]. To take a decision from an economic point of view, it is used to consider a reference value for the discount rate 'e', particularly in Spain, equal to the so-called the Spanish 10-years bond. In the last years, it has always fluctuated below 1%, with an average value near 0.5% [24]. The European policies promote the use of renewable sources, where the NPV is a criterion to be observed [25]. Once the directive was transposed to Spanish legislation, recommended solutions are based on an IRR equal to this reference value plus 3%, such as in [26]. For this reason, the IRR has been selected in this work as an economic indicator or objective. In this way, the final optimal solution must be selected from those with maximums in ES and IRR, with a lower limiting value for IRR, which can be established at about 3.5% to assure the profitability of an installation.

With these principles, a multi-objective optimization method must be performed. The main problem is to satisfy several objectives that come into conflict (an energy improvement can mean a higher economic investment, which damages the profitability of the installation). In this sense, the Pareto optimality method has been proven to be highly effective in reaching the best compromise solution among all the possible cases [27].

249 The classical optimization procedures are based on Newton's method [28],
250 which can be improved in many cases by adopting intelligent optimization techniques,
251 such as GA of ANN [29]. In many cases, these new methodologies present better
252 searching for the optimal solution, diminishing the difficulties associated with ill-
253 conditioned problems, or avoiding weak or local minimums, among other advantages
254 over those conventional methods. There are many reports justifying the accuracy of
255 these methods to proper optimizations for both classical [30, 31] and intelligent [14, 32-
256 34] procedures. The optimization method is selected depending on the computing time
257 to the particular applied model, avoiding a much-extended time required by the
258 computer to finish the process. When the model consumes a little time to run, a high
259 number of iterations can be used, while those, which use complex models (such as 2D
260 or 3D), tend to search for a low number of repetitions.
261 An alternative strategy to optimums searching, based on statistical premises,
262 corresponds to the Design of Experiments (DoE) in order to minimize the number of
263 tests to be carried out (experiments or modeling) [35]. Researchers such as Park et al.
264 [36] optimize the design of a hybrid GSHP system using a DoE. In this case, instead of
265 the Pareto's method, the final solution was selected from the overlaid contour of three
266 surfaces, each one for a single-objective bi-variant function, generated by *Response*
267 *Surface Methodology* (RSM). The three objective functions were the total initial cost,
268 the total present value costs, and the annual energy use, and two decision variables
269 associated with a particular type of control of the device and GHE length. On the other
270 hand, other researches also use this technique with satisfactory results [37, 38].
271 In short, using the FLS model with hourly load demands provides accurate
272 results to determine the temperature evolution in a GHE. However, considering the very
273 long time of evaluation (50 years) and several internal iterations to conciliate the hourly

ground thermal loads with the ground carrier fluid temperature evolution, also limiting this last value, the simulation of any case will require a considerable time to perform all the necessary calculations by a computer. When this model or one similar is used in a multi-objective optimization strategy, it is suspected that the computation time would be excessive due to the many different cases to be evaluated. In order to provide a friendly and relatively fast method for the optimal design of a GSHP, an alternative strategy can be adopted, following two steps:

-Firstly, an appreciable amount of cases with different input factors *IF* (variables) must be simulated, to provide economic and environmental (or energetic) indicators such as NCP-LGE or ES-IRR. For this purpose, a systematic sampling must be done from a DoE, from which several optimums can be observed.

-In a second step, the final decision is taken by selecting the best option among all of them, using the Pareto's optimal approach for the overall multi-objective optimization associated with the GSHP design.

In this paper, a case study for the optimal design of a hybrid GSHP has been applied to an official building located in Andalusia (Spain), where there is a thermal imbalance by ground cooling-dominant load and a surface limitation for the GHE field. It starts from the hourly profile of the building load, establishing an initial installation scheme. Later, a set of experiments over a single vertical borehole determines the thermal ground characteristics and defines the local STGF exclusively for this set-up. From these previous data, a DoE establishes a combination of different input factors, related to borehole geometric characteristics (depth, number of elements, etc.) and control strategies for this hybrid behavior. For each of them, the FLS method is used to simulate the hourly thermal building load for a very long time (up to 50 years), optimizing the GHE behavior to maximize the energy savings (ES) in relation to the

299 conventional operation of the selected HP device, also determining the economic
300 feasibility throughout its IRR. Once all results are provided, the best solution is selected
301 by searching for a compromise between economic and environmental benefits through
302 the Pareto's optimally method.
303
304 **2. Methodology.**
305
306 A procedure for an optimal design of a GSHP system searches for the adequate
307 GHE total length (L_{GHE}), which matches with the best conciliating solution from the
308 energetic/environmental and economic points of view. The main procedures start from
309 the GHE size (L_{GHE}) [8], from which the ground response is evaluated by determining
310 the carrier fluid temperature during the useful life of the installation (usually 25 years).
311 Internal algorithms can be included [18, 20] in order not to overcome the temperatures
312 of 0ºC in winter and 35ºC in summer, which are implemented into the control system of
313 the HP. Among available methods, the analytical procedure is quite friendly and
314 accurate, compared to the numerical ones with high computational costs [7]. Quite
315 differences have been observed among the different analytical procedures [39], being
316 the most advanced ones those that simulate the process with a one-hour sample time.
317 In addition to time-dependent variables (temperatures, heat flows, and so on),
318 final indicators must be extracted from it, such as shave factor (share of building loads
319 provided by GSHP and conventional system: 0% is assumed for conventional ones,
320 while GSHP can reach up to 100%) [16], energy consumption (usually corresponds to
321 electricity), and its economic cost, year by year. From these results, an energetic and
322 economic assessment can be done, providing an investment selection criterion [23], next

to energy savings (and/or environmental ones), when the evaluated case is compared with the conventional case (which does not use GHSP).

For carrying out the optimization procedure, several aspects must be defined: i) some inputs (input factors of decision variables) to the selected model; ii) the characteristics of the outputs from which to take decisions (objective functions, in this work throughout energy-environmental and economic indicators), and iii) decision-making criteria (addition of several objective functions applying weighting factors, searching maximum or minimum, and so on).

In a general way, once selected the energy/economic model into an optimization procedure, the overall process can be summarized as follows:

i) Building load calculation.

ii) Selection of the different devices (HP and dry air cooler) and their characterization.

iii) Thermal ground characterization of the GHE (from experiments).

iv) Multi-objective optimization procedure, from which select the final design.

For the present particular case, the optimization method is based on applying first a Design of Experiments (DoE), which defines a set of simulations subjected to different combinations of input factors. At the end of the simulation stage, all the results are evaluated throughout the Pareto's optimally process, finally selecting the adequate design for the desired objectives.

2.1. System description.

General data, characteristics of devices, and installation are summarized in table 1, from which start the design study (justifications will be provided in the following sub-sections):

i) The building is an official construction, subjected to a 12h/day schedule every day. It presents a yearly heat-dominant building load demand but constitutes, in fact, a ground cooling-dominant case, due to the thermodynamic refrigeration cycle of an arbitrary heat pump (HP). It implies that, every year, the outdoor element of the HP rejects to the external thermal source (conventionally the surrounding ambient) more thermal energy than that absorbed from it.

ii) On the other hand, elements related to the HVAC system also appear in that table to provide those building load demands, adjusted to weather conditions, even for extreme cases.

iii) Finally, the proposal of using a GHE needs a large free terrain surface, which is quite limited. In addition, the common practice of installers in this zone is to make the boreholes with the general characteristics indicated in table 1.

Table 1. Main characteristics of the GSHP system.

	CHARACTERISTIC
Building	Official 1998,05 m^2; Heating: 146MWh/year, 277kW peak; Cooling: 124MWh / 210kW peak
HP Device	CIAT MODEL 400V (X2); Nominal heating: 137.7kW (COPs: 4.39); Nominal cooling: 119.3kW / (EERs: 4.69) Eurovent conditions: 12/7ºC temp. evaporator; 30/35ºC temp. condenser;
Air-to-water heat exchanger	INDITER AWSN-43D; Capacity: 154kW; V_f= 27m^3/h; max. ΔT_f= 5ºC; Pump/Fan Consumption: 1.5/5.8kW
GHE Field	540 m^2 available surface (18m x 30m); Boreholes: 0.15m ϕ_b; U tube 32/40mm ϕ_{int}/ϕ_{ext} PE100; Filling bentonite mix

2.1.1. Building load.

The envelope and inner uses origins a thermal load that has been estimated by an authorised software in Spain [40], which includes the solver DOE-2.2 [41]. Although this software runs with hourly data, the results are only related to cumulated monthly

and seasonal heating and cooling loads. To infer hourly demands from that monthly aggregated energy, a non-linear multivariate regression approach has been carried out, taking into account the climatic variables profile along the year [42]. In addition, in the warm periods where both heating and cooling demands appear, outdoor temperature allows providing the major of these loads (by free-cooling and free-heating). Thus they have been removed from the demands from the HP device in the current study. The final effective load is presented in figure 1.a. The resulting hourly building load $Q_B(\tau)$ (kWh/h) (equivalent to average hourly energy flow in kW units) corresponds to the main input to the developed analysis, which is segregated as average hourly demands of heating $Q_{B,H}(\tau)$ and cooling $Q_{B,R}(\tau)$. An example of the load fraction distribution along a day in winter and summer can be seen in figure 1.b.

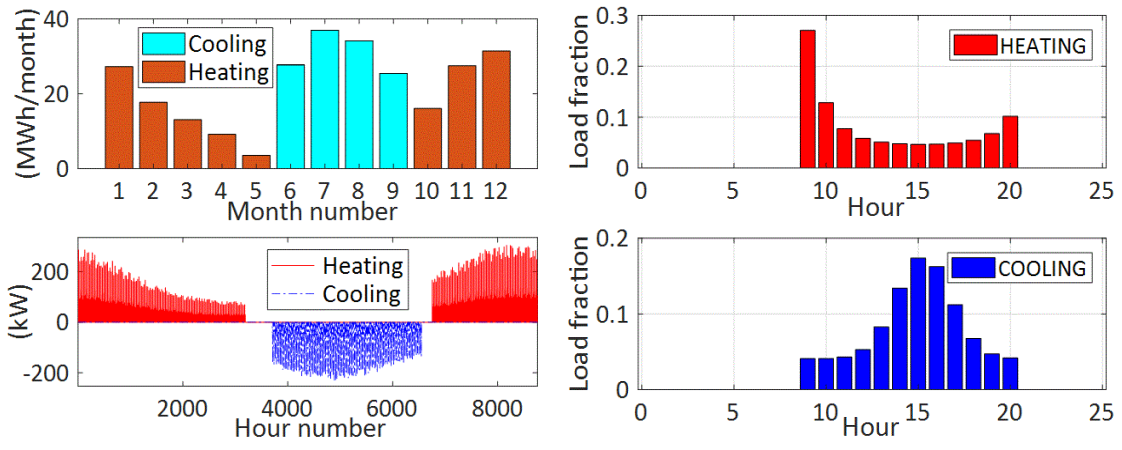

a) b)

Figure 1. Building load: (a) initial; (b) final demands removing free heat exchanging periods.

2.1.2.- Devices and their characterization.

Considering the HP efficiencies (see table 1) and building thermal load profiles (see figure 1), a ground cooling-dominant case is identified. It presents a yearly average ground heat load or imbalance of 4.59kWt (average net load to be injected to the ground

391 by the GHE, as a result of subtracting the heat injection in summer and extraction in
392 winter), and a highest average monthly ground load of 60.38kW (in July). The peak
393 hourly load at the external devices of the HP in summer corresponds to 259kW. Due to
394 this high value, it is necessary to use a secondary device at extreme periods, although its
395 utilization factor will be quite low. As only the main device is attached to the GHE, the
396 peak hourly ground load is 168kW (from which it has been decided the model of air-to-
397 water heat exchanger). From evaluating the building and ground loads, the yearly shave
398 factor that this installation can reach is 89.08% (91.2% in winter and 86.6% in summer).
399 The scheme of the installation is shown in figure 2. A W-W-HVAC system has
400 been selected to cover the indoor loads, including two HPs in parallel. The main one
401 provides the major building load $Q_{B,GHE}$, by connecting it with the GHE, supporting the
402 ground load Q_{GROUND}. The auxiliary one takes over the building peaks $Q_{B,aux}$ making
403 use of an air-to-water heat exchanger, interchanging the corresponding ambient load
404 $Q_{AMBIENT}$. In this way, the outdoor thermal sources correspond to the ambient for the HP
405 attached to the air-to-water heat exchanger, and to the ground (up to 150m deep) for that
406 main device connected to the GHE. For this last case, the ground temperature far from
407 piles tends to be constant throughout the year. Thus the HP efficiencies are better than
408 for the heat exchanged with the ambient, resulting in lower energy consumption [43].

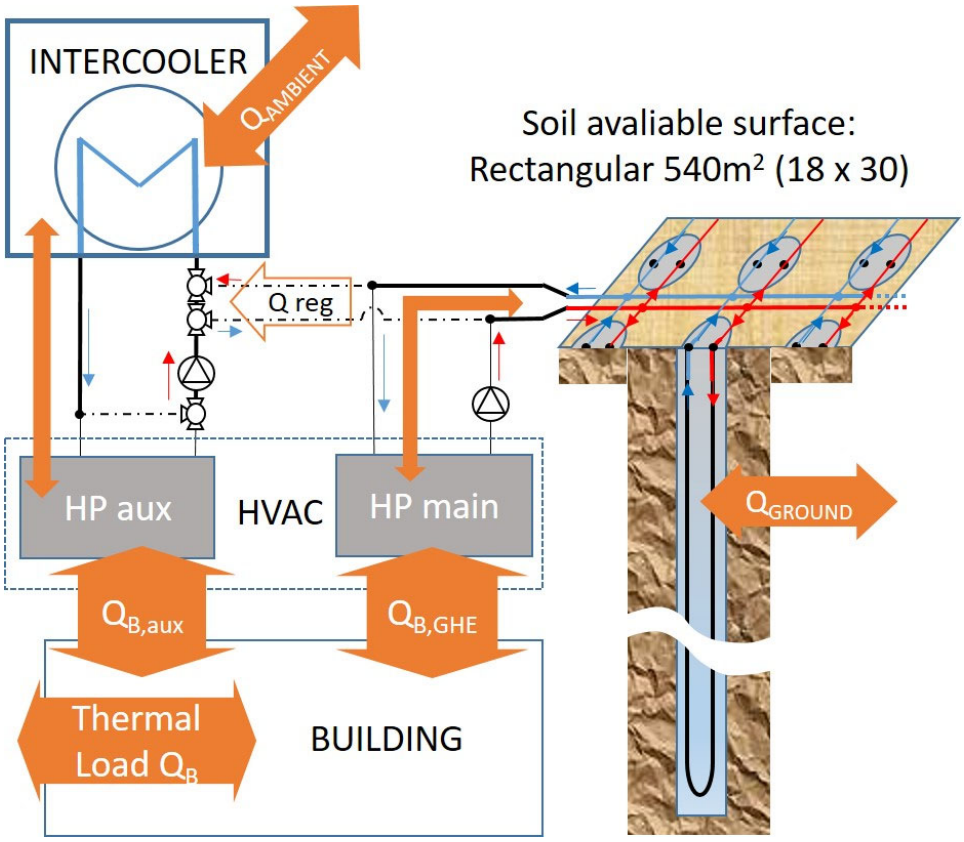

Figure 2. Scheme of hybrid HVAC-GSHP installation.

Several fluid circuits can be observed in figure 2. The gross lines represent the pipes through which fluids constantly circulate. Completing the closed circuits for the regular operation, the tubes appear connected to those denoted with thin continuous lines. However, this intercooler also has a complementary assignment during regeneration periods (at night, without human activity in the building), which consists of heating (in winter) or cooling (in summer) the ground by transferring the load Q_{reg} to the ambient. For this purpose, three 3-way controlled valves have been included in its external circuit. The regeneration circuit connects the primary tubes (gross lines) with those depicted by dash-dot lines, by means of the indicated valves. In this case, only the auxiliary pump operates.

Considering the characteristics of HP and air cooler in table 1, an energy balance provides the maximum carrier fluid temperature variation ΔT_f at the outdoor unit of the HP (evaporator in winter and condenser in summer) around 5ºC at full load in summer.

For the most unfavourable scenario, a constant value of 5ºC has been assumed for this term, thus providing a maximum uncertainty over the calculation following procedure.

As the efficiency of the HP varies with carrier fluid temperature, its instantaneous behavior over time is quite important to be known. Therefore, to assure reliable results, a function of the partial and full load HP efficiencies for heating and cooling has been incorporated into the study. For this purpose, data provided by the manufacturer relate the flow rates at the evaporator (Q_{ev}), condenser (Q_{cond}), and electrical power at the compressor (W_c) with the outlet temperatures of the carrier fluid from both the evaporator ($T_{ev,out}$) and condenser ($T_{cond,out}$). From them, the corresponding efficiency values have been extracted firstly, one for the COP (for heating, equal to Q_{cond}/W_e) and another for the EER (for cooling, equal to Q_{ev}/W_e). Later, a corresponding binomial function was deduced for their instantaneous behaviour: $COP \approx f_1(T_{cond,out},T_{ev,out})$ and $EER \approx f_2(T_{cond,out},T_{ev,out})$, with the tendencies shown in figure 3.

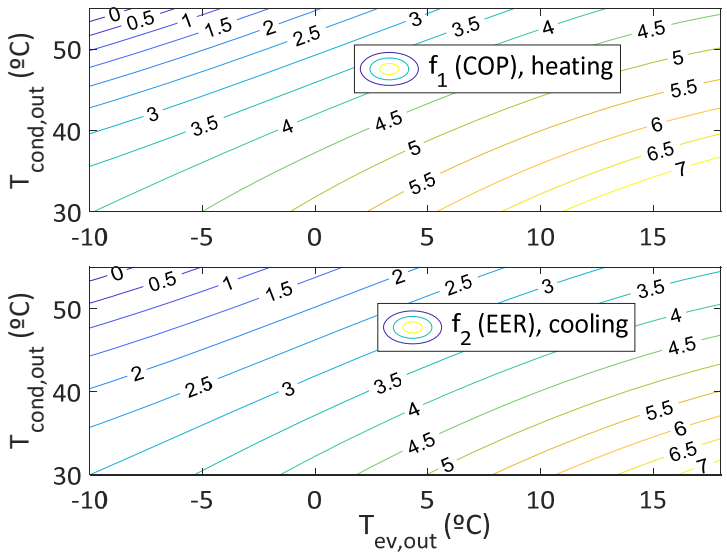

Figure 3. Responses surfaces of f_1 (COP) and f_2 (EER) for the evaluated Heat Pump.

In winter, the external device of the HP acts as the evaporator. Thus $\Delta T_{ev} = \Delta T_f$ corresponds to that increment at the GHE field. On the contrary, $\Delta T_{cond} = \Delta T_f$ in summer. In any case, the internal elements of the HP provide to the fluid the temperatures at nominal conditions for each season, as recommended by the manufacturer (40/45ºC for heating loads and 7/12ºC for cooling loads). These relations make it possible to establish the equalities in eq. (1):

$$Winter: \quad T_{ev,out} = T_{f,av} - 0.5\,\Delta T_{ev} = T_{f,av} - 0.5\,\Delta T_f$$

$$Summer: \quad T_{cond,out} = T_{f,av} + 0.5\,\Delta T_{cond} = T_{f,av} + 0.5\,\Delta T_f \qquad (1)$$

2.2. GHE field and characterization.

The GSHP is constituted by the previous elements, adding a boreholes field that forms the GHE to interchange those heat rates with soil, with the characteristics shown in table 1, corresponding to the common practice of installers in this zone. The limited surface for the GHE field makes it necessary to define an optimal disposition of elements among several possibilities for a number of boreholes between 18 and 24, placing them in a rectangular or quincunx shape (r/q). These shapes adapt better to the limited disposal of annexed terrain surface to the building, as shown in table 1. Therefore, the initial objective of a design procedure is searching for the adequate total length of the overall GHE field, L_{GHE} (m), (as a result of multiplying the number of elements N_b and their depth H (m)), considering the possible disposition r/q and the thermal characteristics that must be determined.

For the thermal characterization of the terrain (including hole filling material and soil), a single pile is first built, drilling the terrain, inserting the U-tube, and filling the well with a special cement based upon bentonite and the pipe with the carrier fluid. A

469 little time is allowed for the fluid to reach the temperature of the surrounding ground.
470 Then, a developed device for this purpose carries out two experimental tests [22]:
471 Firstly, an undisturbed Ground Temperature Test (GTT) is developed, to obtain
472 the average value for the soil temperature T_s (ºC), which will be supposed to remain
473 constant along time far from each borehole, serving as a thermal source. The procedure
474 consists of measuring the outlet temperature of the pipe from the grout as the carrier
475 fluid is circulated in laminar regime (mean velocity of 0.05 m/s giving a Reynold's
476 number, *Re*, around 1800) in order to assure that its temperature is the same as that
477 corresponding to the ground. It provides its profile with the depth, from which the
478 average value T_s is calculated [44].
479 Later, a three-day Temperature Response Test (TRT) is put into practice,
480 injecting a constant 4000 W heat rate, corresponding to a unitary heat pulse q_0 of 36.36
481 W/m (from an experimental borehole depth of 110 m), and with a volumetric flow of 15
482 L/min (turbulent regime with 11400 *Re*), providing the time dependent profiles of inlet
483 and outlet fluid temperatures versus the trial, denoting its mean value as T_{f0} (ºC) [21].
484 From this experiment profile, the ILS method was used to identify some thermal
485 characteristics of the ground such as the ground thermal conductivity λ_s (W/m·K) and
486 volumetric heat capacity C_S (J/m^3·K) [45], given the grout radius r_b (m) and the
487 effective borehole thermal resistance R_b (m·K/W), which must be estimated by an
488 auxiliary model [46]. As the experimental device assures a constant value for the heat
489 pulse during the test, T_{f0} follows a linear tendency of the natural logarithm of time at the
490 end of the experiment, as eq. (2) shows:
491
492 $$T_{f0} = a + m\ln(\tau)\ ;\ m = \frac{q_0}{4\,\pi\,\lambda_s}\ ;\ a = T_S + q_0\,R_b + \frac{q_0}{4\,\pi\,\lambda_S}\left[\ln\left(\frac{4\,\alpha_s}{r_b^2}\right) - \gamma\right] \quad (2)$$
493

where α_S (m^2/s) denotes the soil thermal diffusivity, and γ corresponds to the Euler's constant. The term λ_s is obtained first from the slope of the straight-line *m*, and later, diffusivity is derived from the constant value *a*, providing then C_S, throughout the relation $\alpha_S = \lambda_S / C_S$.

In order to model the heat exchange in the GHE field for the design purposes of the present study, the FLS method simulates the evolution along time τ_i (being '*i*' the hour number, finishing the 50 year-period at the hour $k = 50 \cdot 365 \cdot 24$) of the average fluid temperature of the GHE $T_{f,av}$, subjected to a superposition of piecewise linear step heat inputs in time, derived from the heat pulses $q_i(\tau)$ (W/m) [13], as eq. (3) shows:

$$T_{f,av} = T_S + \frac{1}{2\,\pi\,\lambda_S} \sum_{i=1}^{k} \left\{ (q_i - q_{i-1})\; g_{\,GHE} \left(\frac{\tau_i - \tau_{i-1}}{\tau_s} \right) \right\} + R_b \sum_{i=1}^{k} (q_i - q_{i-1}) \qquad (3)$$

Apart from incorporating *Ts*, λ_s, and R_b, $q_i(\tau)$ terms are initially determined from the hourly building load, HP efficiencies, and L_{GHE} , that is:

$$q_{i,H}(\tau) = \frac{Q_{B,H}(\tau)}{L_{GHE}} \left(1 - \frac{1}{f_1}\right) \qquad (3.1)$$

$$q_{i,R}(\tau) = \frac{Q_{B,R}(\tau)}{L_{GHE}} \left(1 + \frac{1}{f_2}\right) \qquad (3.2)$$

The key component of this expression corresponds to the *g-function*, as the thermal response factor of the GHE, which depends on a combination of the number of piles (N_b), depth (*H*), and disposition (*r/q*) [9, 10]. A long-term period *g-functio*n (LTGF) profile for a single borehole can be derived by a time-dependent analytical function subjected to α_s, H and ϕ_b [12]; going forward of the methodology established previously by Eskilson's approach [10], who obtained it first numerically. This approach could be

518 enough for design purposes when peak loads were not considered. However,
519 developments demonstrated also that intermittent heat transfer by short cycles of
520 operation at vertical GHE improves their effectiveness [6, 43]. Thus models must
521 include the transient behaviour of the borehole at the first stages of any arbitrary heat
522 pulse, beyond the one represented by R_b, which does not consider the thermal capacity
523 of the grout. For this reason, a complementary short-time *g-function* (STGF) must be
524 evaluated to build a single borehole *g-function*.

525 In this sense, Yavuzturk and Spitler [13, 47] extended the Eskilson's method by
526 applying eq. (3) to a single unitary heat pulse q_0 to provide the STGF by solving the
527 expression of eq. (4), generating T_{f0} synthetically throughout a 2D numerical model for
528 a given steady-state time $\tau_s = H^2/9 \cdot \alpha_S$, and a T_S previously established.

529

530 $$g(\tau_{dim}, r_{dim}) = \frac{2\,\pi\,\lambda_S}{q_0}\,\left(T_{f0} - T_S + q_0\,R_b\right)\;;\;\tau_{dim} = \frac{\tau}{\tau_S}\;;\;\; r_{dim} = \frac{r}{H} \qquad (4)$$

531

532 Recently, the authors demonstrated that eq. (4) can also be used to obtain this
533 STGF but determining T_{f0} and T_S experimentally from GTT and TRT tests [15],
534 extending the capabilities of TRT to provide short-time information about a single
535 vertical GHE. This procedure was validated by matching model results with a set of
536 quite demanding heat pulse cycles in a short-term, where a high accuracy was proven.

537 In short, the global characterization of a single borehole starts from both the
538 GTT and TRT tests and then, by solving the ILS method of eq. (2) the analytical
539 approach for LTGF and the experimentally based determination of STGF at eq. (4).
540 These two last components provide a precomputed complete thermal response factor for
541 all the time in a single borehole. From this, the overall function for a GHE field with
542 several grouts must be constructed considering N_b, H, and r/q, with adequate separation

543 distances between them into the available GHE surface, and finally applying the
544 superposition principle in space.
545
546 *2.3. Energy and economic analysis procedure.*
547
548 The model described in this section determines, as a last resort, the energy and
549 economic savings (output variables) from operating the GSHP system subject to a
550 combination of certain varying input factors (IF), which will be explained later. The
551 output variables are presented for a 50-year period, corresponding to annual and global
552 percentages for energy savings ES (%), shave factor SF (%), and internal rate of return
553 of the investment IRR (%). Annual energy indicators have been evaluated from the
554 integration of the hourly-step analysis of the system. From these annual cumulated
555 energy results, an economic assessment is done, providing their savings and the IRR.
556 The energy analysis uses the eq. (3) to evaluate the heat transfer throughout the
557 GHE field, simulating the evolution of $T_{f,av}$. Since the hourly evolution during a year of
558 the building load is considered the same for all the period studied (50 years), the load
559 transferred to/from the ground changes from one year to another depending on several
560 tasks, making necessary a detailed assessment along all the period. These tasks are as
561 follows:
562 i) The HP efficiencies (COP for heating, approached by the surface
563 function $f_{COP}(T_{cond,out},T_{ev,out})$ and EER for cooling by that
564 $f_{EER}(T_{cond,out},T_{ev,out})$), were previously fitted (as can be observed in Figure
565 (3) and are closely subjected to $T_{f,av}$, as eq. (1) showed.

ii) A key factor to optimize the installation establishes set points (upper and lower limits) for the fluid temperature, $T_{f,U}$ and $T_{f,L}$, in order to maximize these efficiencies [20].

iii) The maximum thermal load of the device to be transferred: a maximum $Q_{B,Hmax}$ (winter) of 137.7kW is initially assumed, since for $Q_{B,Rmax}$ (summer), it corresponds to 119kW (nominal conditions). But these load peaks may produce the $T_{f,av}$ to overtake those mentioned temperature limits ($T_{f,U}$ and $T_{f,L}$). They must be prevented.

iv) For this same purpose, another strategy consists of including a regeneration cycle [20] by extracting (or injecting) a certain heat flow during several hours in a day ($N_{reg,H}$ and $N_{reg,R}$ for heating and cooling seasons, respectively). It corresponds to another key factor in the global model of the GSHP system. The Q_{reg} (W) could correspond to the maximum capability of by the air-to-water heat exchanger (154kW, see table 1). From a sensitivity analysis of this system, it has been concluded that those terms for heating demands ($T_{f,L}$ and $N_{reg,H}$) are not necessary to be changed, always assuming a 2ºC value for $T_{f,L}$ and no regeneration is needed at winter season ($N_{reg,H} = 0$).

Thus, the variable input factors to the model (IF) correspond to: the number of boreholes N_b and depth H, disposition of them into the GHE field (rectangular or quincunx, r-q), and the control strategy factors $T_{f,U}$ and $N_{reg,R}$. These inputs together with some pre-processed terms (such as the hourly building load, HP characteristics, T_s, λ_s, R_b and g-function, Q_{reg}, terms at f_{COP} and f_{EER} surface functions related to HP efficiencies), act as input variables to the algorithm presented in figure 4.a, in order to

591 determine the desired cumulative results: yearly and overall period loads and
592 consumption, differentiating between winter and summer seasons. To obtain these
593 cumulative results, it is necessary to evaluate the hourly GHE behavior firstly during a
594 very long time, resulting in: $T_{f,av}(\tau)$, $COP(\tau)$ and $EER(\tau)$, $W_{c,H}(\tau)$, $W_{c,R}(\tau)$, $Q_{B,H}(\tau)$ and
595 $Q_{B,R}(\tau)$ supported by the GHE, avoiding to exceed the fluid temperature limits
596 throughout the boreholes.
597
598

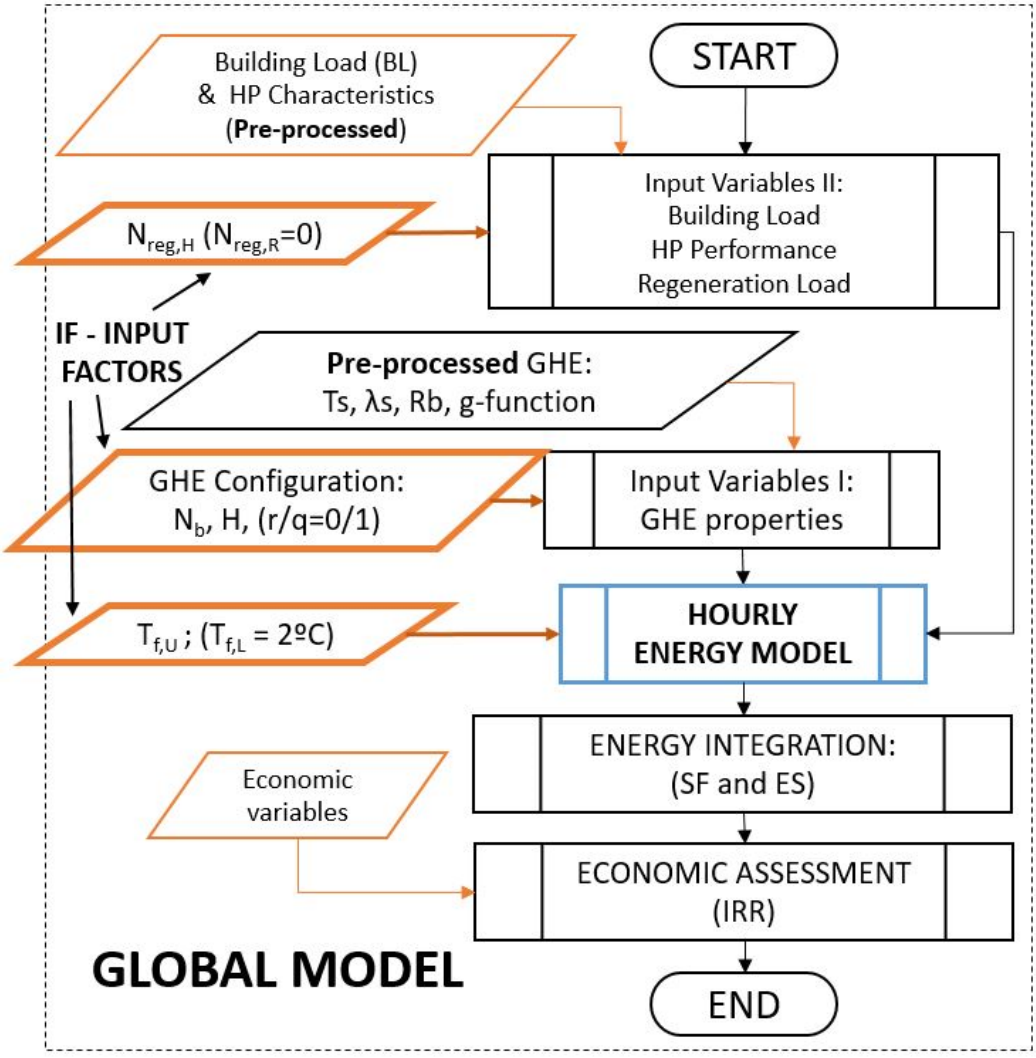

599
600 a)

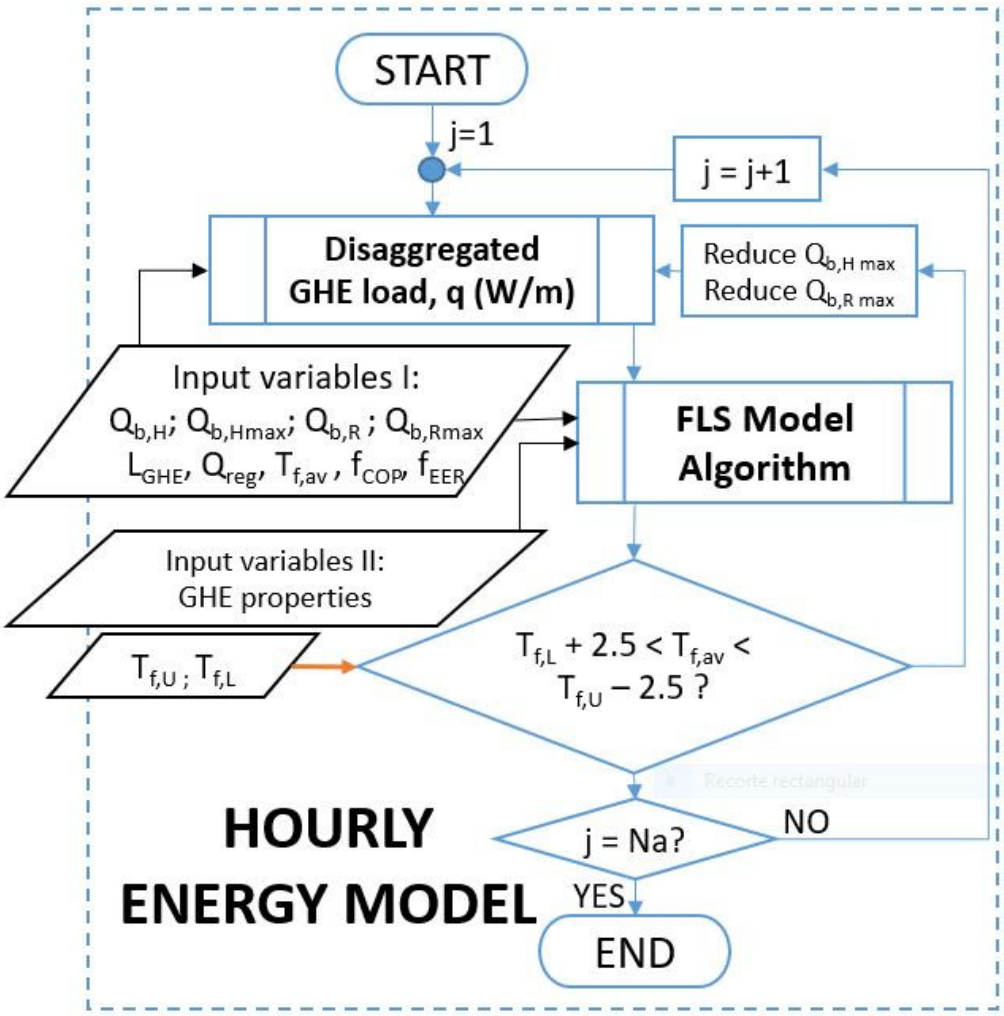

b)

Figure 4. Mathematical model of GHSP behavior: a) Global Procedure and b) Hourly Energy Procedure.

For this purpose, the hourly simulation procedure (see "HOURLY ENERGY MODEL" in figure 4.a, which develops the algorithm in figure 4.b), decomposes first the overall period on yearly calculations, starting with $Q_{B,H}(\tau)$, $Q_{B,R}(\tau)$ and also considering $Q_{B,H\ max}$ and $Q_{B,R\ max}$ (taking initially the values 137.7kW and 119kW, respectively). This algorithm fixes the bounds $Q_{B,Hmax}$ and $Q_{B,Rmax}$ (which can change from one year to another) that avoids trespassing $T_{f,av}$ limits ($T_{f,L}$ and $T_{f,U}$), by evaluating the generated $T_{f,av}(\tau)$ profile from the "FLS model algorithm" (see it in figures 4.b): if any of the $T_{f,av}$ limits are exceeded, the initial constraints $Q_{B,Hmax}$ and

$Q_{B,Rmax}$ are a 3% diminished. New $Q_{B,H}$ and $Q_{B,R}$ profiles appear, where the absolute maximums are slightly lower than before, and the procedure starts again. Once those objectives are reached for one year, the process continues with the following one until the end of the overall period of study (50 years).

The procedure for evaluating the annual energy balance included in the previous algorithm is as follows (see "FLS Model Algorithm" in figure 4.b): given an initial $T_{f.av}$ along the current year, eq. (1) establishes the values entering and leaving the external device of the GSHP ($T_{ev,out}$ in winter and $T_{cond,out}$ in summer), while the corresponding ones to the internal exchanger are fixed, depending to the season ($T_{cond,out}$ = 40ºC in winter, and $T_{ev,\,out}$ = 12ºC for summer). The previous fitted surface functions, $f_{COP}(T_{cond,out},T_{ev,out})$ and $f_{EER}(T_{cond,out},T_{ev,out})$, determine the COP(τ) and EER(τ) values along time during that year. In addition, $Q_{B,H}(\tau)$ and $Q_{B,R}(\tau)$ provide the load to be exchanged by the GHE, $q_{i,H}$ and $q_{i,R}$ (for annual hours i = 1 to 8760) throughout eqs. (3.1) and (3.2), respectively. An additional term $q_{j,reg}$ = - Q_{reg}/L_{GHE}, is superimposed in time to the profile $q_{i,R}(\tau)$, related to the regeneration cycles in summer, into a night schedule (during a number of hours, from j = 0 to N_{reg}). In addition, the HP compressor consumption at each instant ($W_{c,H}(\tau)$ and $W_{c,R}(\tau)$), is also evaluated, by dividing $Q_{B,H}(\tau)$ and $Q_{B,RH}(\tau)$ into their corresponding efficiencies. Then, a $T_{f,av}(\tau)$ profile is determined from eq. (3). It generates new conditions about $T_{cond,out}(\tau)$ and $T_{ev,out}(\tau)$, establishing new COP(τ) and EER(τ) profiles, and consequently, $q_{i,H}(\tau)$ and $q_{i,R}(\tau)$, from which to evaluate newly $T_{f,av}$ by eq. (3). This procedure is repeated until that annual $T_{f,av}$ profile does not change between iterations. At this point, it is important to remark that the FLS model evaluation during one year implies an initial $T_{f,av}$ profile beyond the year under study due to the superimposing of heat pulses at eq. (3), that enlarges until the end of the overall period. This profile will serve as initial curve of the $T_{f,av}$ to start the iterative

638 procedure described here for the following year. For the first year, this initial $T_{f,av}$ is
639 considered constant and equal to T_s.
640 Once the hourly analysis from the previous algorithm is developed and
641 following the general procedure in figure 4.a, results are cumulated by year 'j' (from 1
642 to 50). In relation to the energy saving eS (MWh/year), it corresponds to the difference
643 between the cumulated value $W_{c,j}$ (MWh/year), and that one $W_{c0,j}$ (MWh/year) with
644 supported loads by a conventional way (heat exchanging of the external HP device with
645 the ambient, as a result of dividing each seasonal cumulated building load $Q^j_{B,H}$ and
646 $Q^j_{B,R}$, by the corresponding seasonal efficiency of the device working at nominal
647 conditions, COP^j_s and EER^j_s, provided by the manufacturer). For each year 'j', energy
648 saving (in energy units eS, and in percentage ES) can be obtained from eq. (5):
649
650 $$eS^j[MWh/year] = \left(\frac{Q^j_{B,H}}{COP^j_s} - W^j_{c,H}\right) + \left(\frac{Q^j_{B,R}}{EER^j_s} - W^j_{c,R}\right); \quad ES^j(\%) = 100 \cdot \frac{eS^j}{W^j_{c,H} + W^j_{c,R}} \quad (5)$$
651
652 If any of the limits $Q_{B,Hmax}$ and $Q_{B,Rmax}$ are lower than the initial ones (137.7kW
653 and 119kW, respectively), the cumulative energy exchanged with the ground will be
654 lower than the maximum possible, providing then the shave factor SF by dividing those
655 cumulated values.
656 From these energy savings, the corresponding economic savings can be
657 evaluated considering the electricity cost c_e (€/kWhe). For the current year, 2020, it is
658 around 0.115 €/kWhe (taxes included) according to the regulated market and whose
659 prices are indicated in the Red Eléctrica de España organization (REE) [48]. In addition,
660 the investment cost, I_{GHE} (m.u.), is calculated by adopting, for a N_b and H, a fixed cost
661 of 500 €/borehole, next to a variable drilling cost of 20 €/m deep, as well as 2000€ of

auxiliaries, usual data for this geographic zone. The initial cost is then increased up to 40% due to installation and labor costs [18].

The economic assessment is carried out from these two data, as well as $\overline{eS}$ (the mean value, for all the period, of eS^j) next to the annual increment of prices of this type of energy Δce (dimensionless) [23]. Because of this, the internal rate of return (IRR, %) is determined, since it corresponds to a very useful indicator of the profitability of the solution. It corresponds, in percentage, to the discount rate 'e' (dimensionless) which assures a zero Net Present Value (NPV) at the end of the installation useful life (N_L), as eq. (6) shows:

$$NPV = 0 = \overline{eS} \cdot c_e \cdot \sum_{j=1}^{N_L} \left[\left(\frac{1+\Delta ce}{1+e} \right)^j \right] - I_{GHE} \quad (6)$$

From this equation, the payback period PB can also be estimated, deducing the number of years where NPV is equal to zero (and obviously different from N_L), for this discount rate related to that current Spanish 10-years bond (e = 0.005). In particular, a simple payback period SPB can be calculated as the ratio of investments I_{GHE} and economic savings for the first year ($eS \cdot c_e$), by not considering year-to-year price changes.

2.4. Optimal Design Procedure.

For an optimal system design, there is a need to assess the GHSP behavior using the described previous procedure, which assigns different values to the input factors (*IF*). A Design of Experiments (DoE) must establish several combinations between them. This statistical technique analyzes, with the minimum number of experiments, the response of a system (output variable) depending on several parameters (input variables

687 or factors) which guide its behavior, trying to obtain the maximum possible information
688 about the process [49]. Particularized for this study, the type of design will be full
689 factorial (FFDoE): the responses are measured for all combinations of factor levels,
690 providing detailed information but without redundant experiments, evaluating direct
691 effects of the factors on the output, as well as interactions between those factors [50].
692 The output variables or responses under study correspond, in this case, to the indicators
693 ES and IRR.

694 Input factors must include values into an adequate number of levels, related to
695 the spatial disposition, a coherent range for the number of boreholes N_b, grout depth H,
696 maximum temperature to be reached by the fluid $T_{f,U}$, and the number of daily hours to
697 regenerate the soil in summer, $N_{reg,R}$. An adequate design must be found to avoid
698 overloading in the number of simulations, limiting the levels to define. Characteristics
699 of the DoE are summarized in table 2, where the values of the different combinations of
700 the input factors in *IF* by this FFDoE can be observed. The space limitations to
701 distribute the different drillings for the GHE due to the disposal surface, considering an
702 adequate separation distance between boreholes, justify two spatial dispositions to be
703 evaluated, (rectangular and quincunx), also establishing a four-level factor related to the
704 number of piles, N_b, into a range of 18 and 24. These dispositions can be observed in
705 figure 5. In addition, experience recommends affordable deeps between 80 to 140m for
706 H, using a seven-level factor. For each of the 56 resulting configurations, a *g-function*
707 must be generated from a previous single borehole *g-function* after ground
708 characterization (connecting both STGF and LTGF functions). In addition, the yearly
709 unbalanced thermal load produces the ground temperature to rise over time, so it must
710 be limited. For this purpose, another two factors must be included in the *IF* matrix: $T_{f,U}$

711 in a range between 30 and 50ºC and $N_{reg,R}$ in a range from 0 to 6 hours, adopting four-
712 level values for each of them.
713
714 **Table 2**. Characteristics of the FFDoE applied to the model input factors

Factor	Range	Nr. Levels (*values*)
r/q (qualitative)	Rectangular /Quincunx	2 (*r/q*)
N_b (number)	18-24	4 (*18-20-22-24*)
H (m)	80-140	7 (*80-90-100-110-120-130-140*)
$T_{f,U}$ (ºC)	30-50	4 (*30-37.5-45-52.5*)
$N_{reg,R}$ (h/day)	0-6	4 (*0-2-4-6*)

715

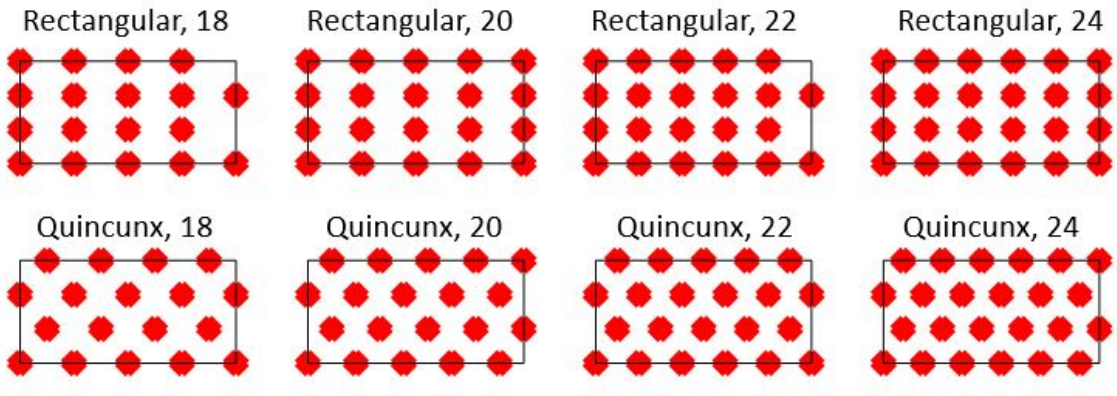

716

717 **Figure 5.** GHE configurations into the limited surface of 540m^2 (30mx18m).

718

719 This design implies 896 combinations of input vectors to run the global model
720 summarized in figure 4. For each combination of factors, the system must be modelled
721 along time for 50 years, obtaining the main indicators about ES and IRR. Applying
722 other techniques of optimization or identification (both based on Newton's method or
723 intelligent techniques) to non-multidimensional models, such as the present one, usually
724 require near or more than 1,000 simulations [32, 33, 51]. As the present case does not
725 reach this value, an affordable computing time can be considered, which considerably
726 reduces the possible cases to be evaluated compared to those applications. Furthermore,
727 possible problems concerning local or weak minimums, which may increase the number
728 of iterations without significant improvements in the results, can be removed.

These results will serve to make a final decision based on the Pareto's optimal solutions, which has already been used with satisfactory results [16, 32, 33]. As a result of all the simulations, a set of cases will appear, being each one a potential candidate to be an optimum. All of them constitute the so-called Pareto front, from which the optimal design case must be selected, depending on the decision-making criteria. Nevertheless, there are no simple rules to making decisions, so the engineer's experience is crucial to take them. Usually, it comes from defining a weighting coefficient for every objective (in this case, corresponds to normalized ES and IRR), being proportionally added to obtain the global objective function to consider in the optimization process. Following the suggestion of other researchers, an equal-weighted coefficient has been adopted in this work to find the final point, in order to give the same importance to both indicators. The procedure will be graphically explained in the following section.

3. Results and discussion.

Once analyzed the building thermal loads and selected and characterized the HVAC devices, this section presents the rest of the design stages sequentially, starting from experimental tests in a single borehole to characterize the ground and the generation of the different *g-functions*. Later, the thermal response along time for all the input factor combinations established by the proposed FFDoE will be simulated, providing both ES and IRR indicators as objective functions. Finally, the results will be analyzed to provide the optimal solution.

3.1. Characterization and preliminary designs.

To make this first important step, the GTT (providing an average of 16.2ºC for T_s) and TRT tests have been performed. Results of the fluid temperature profiles can be seen in figure 6. After that, Zeng's model [46] and the ILS method throughout eq. (2) provides the thermal characteristics indicated in table 3.

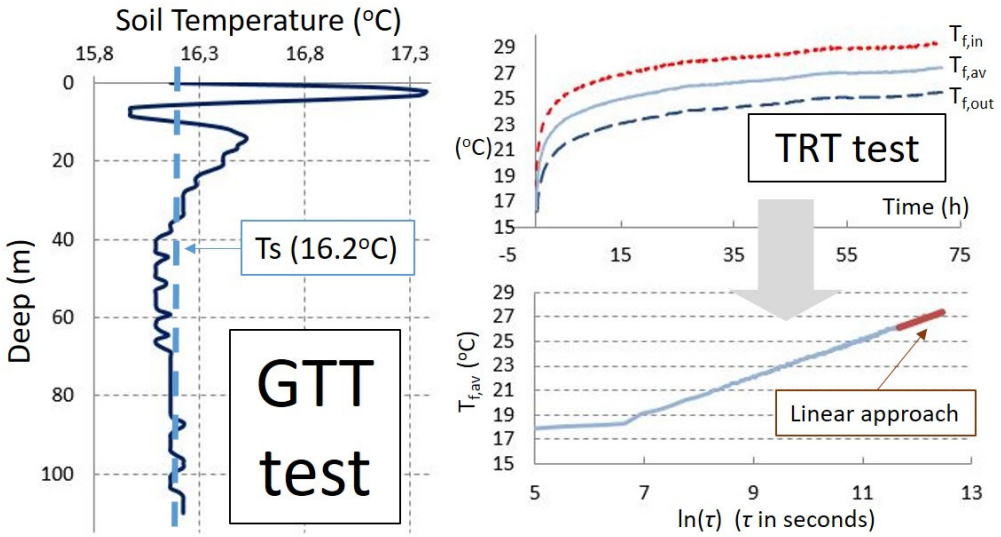

Figure 6. GTT and TRT profiles.

Table 3. Ground thermal characteristics from GTT and TRT.

THERMAL CHARACTERISTICS
T_s= 16.2ºC; λ_s=1.77W/m·K; C_s=1.96MJ/m^3·K; α_s = 9.03·10^{-7}m^2/s; R_b= 0.109 m·K/W

Next, the experimentally based STGF and analytical LTGF for a single borehole are generated and attached, as figure 7.a shows. After applying the superimposition principle in space, the complete GHE *g-function* can be derived. A PC performs all these pre-computing steps in less than 30 minutes. As an example, figure 7.b shows the overall *g-function* for the field composed of 20 boreholes in a rectangular disposition, for different grout depths. As it can be seen, up to about 250h, all these functions are the same (a little further from STGF limit) due to the absence of interactions among piles (a

heat pulse into one borehole does not represent influence over others). Later, the LTGF's for the different GHE dispositions diverge.

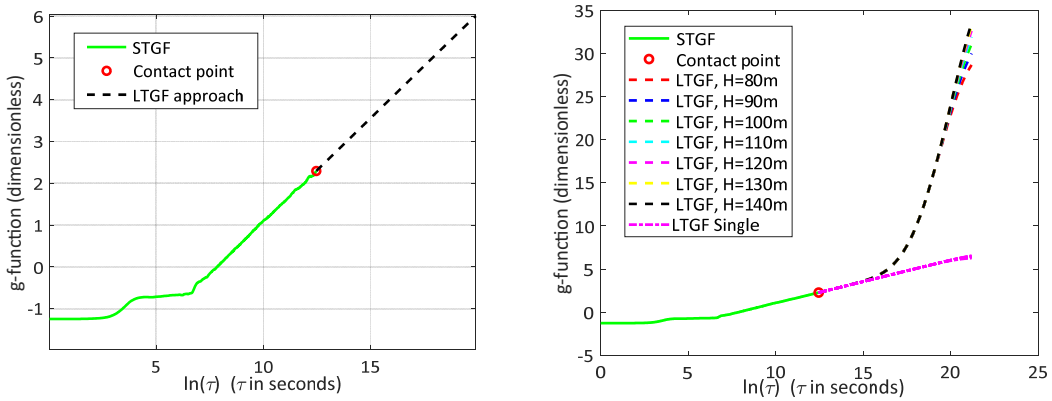

a) b)

Figure 7. Construction of g-function: a) for a single-borehole experimented; (b) for an overall GHE g-function in rectangular disposition for 20 boreholes at different depths.

3.2. Implemented model results from DoE and optimal design selection.

From the defined DoE for the set of IF, the simulations were carried out in around 24 hours on a PC. Partial results have been presented in figures 8 and 9. For a particular GHE field configuration (rectangular disposition of 18 boreholes, 120m deep), figure 8.a shows the evolution along time of COPs and $T_{f,av}$ during several years (the same tendencies are repeated for all the extended period, with little differences), and yearly energy savings (see figure 8.b) for the entire 50-years period. Figure 8.a shows that the final evolution of $T_{f,av}$ does not exceed 35ºC, as the input variable $T_{f,U}$ has been imposed at 37.5ºC. To assure this, the hourly energy model (see figure 4.b) reduces a 3% the supported load by the GHE from the year where this temperature is

reached until the end of the simulation period, iterating until this circumstance is assured.

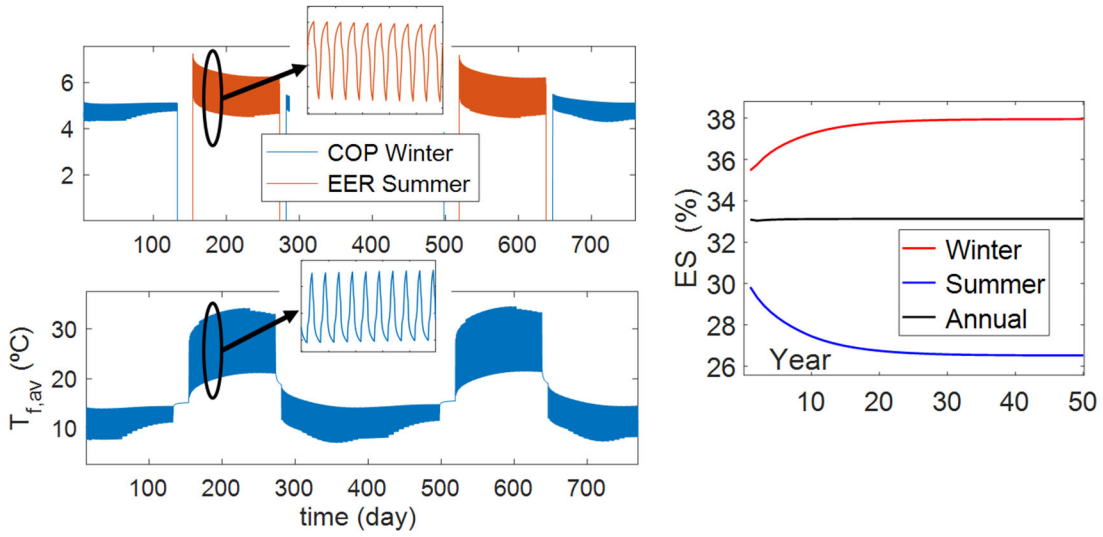

a) b)

Figure 8. Energy model results for rectangular disposition 18 boreholes, 120m deep, $T_{f,U}$ = 37.5ºC and $N_{reg,R}$ = 0: a) Hourly results and b) Yearly cumulative results along period on study.

For this case, a shave factor of 89% is supported by the GHE (91.2% in winter heating, and 86.6% in summer cooling), providing 33.12% of energy savings. This avoided final consumption corresponds to the same saving percentage for both non-renewable primary energy and greenhouse gasses. As it can be seen, ES^j remains practically constant along the period; thus, their mean value $\overline{ES}$ can be assumed as the same as any of them.

This situation corresponds to the highest values for IRR and ES, which depend on $T_{f,U}$ and $N_{reg,R}$, as figure 9.a shows (where $T_{f,U}$ = 37.5ºC, and $N_{reg,R}$ = 0). These factors are repeated as the optimums for all the cases by combining GHE disposition, N_b and H, being demonstrated that this regeneration option is the less useful. Furthermore, the system always runs with the best overall efficiency by limiting $T_{f,U}$ to this value,

diminishing the sharing load of GSHP, instead of consuming additional energy at the air-cooler pump at regeneration periods. In addition, the borehole fluid temperatures take values accordingly to the most efficient operating conditions of the HP. On the other hand, analyzing the best results for one configuration with a depth (rectangular field of 18 boreholes, $T_{f,U}$ = 37.5ºC, without regeneration) between 80 and 140m, figure 9.b depicts that the best economic indicator corresponds to a minimum borehole depth (80m), while the highest energy savings are related to the maximum depth (140m). Newly, the same tendencies have been observed for the rest of GHE configurations.

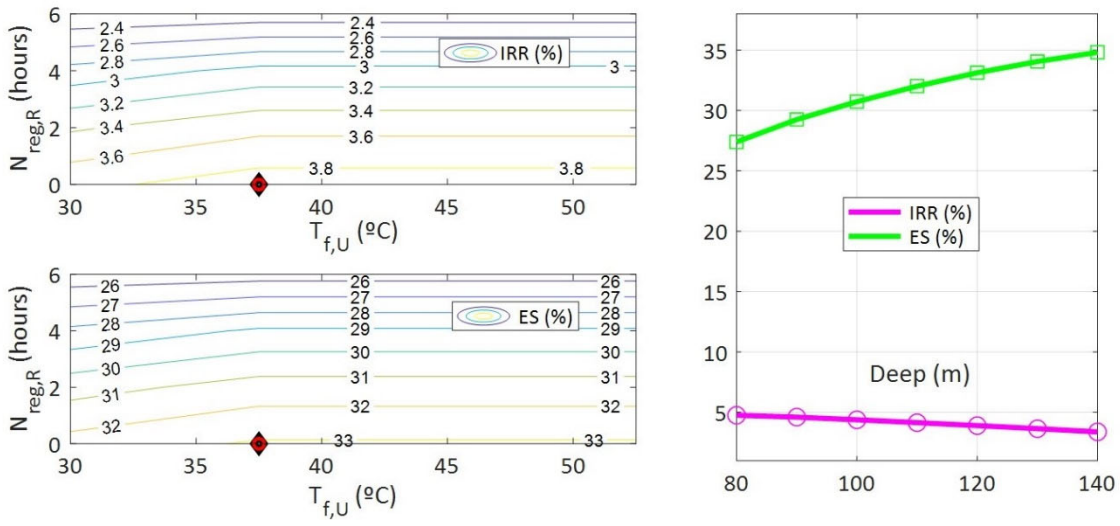

Figure 9. ES and IRR partial optimum solutions for rectangular disposition 18 boreholes: a) Constant surfaces for 120m deep, depending on $T_{f,U}$ and $N_{reg,R}$; b) The best values of $T_{f,U}$ = 37.5ºC and $N_{reg,R}$ = 0, depending on H (m).

These contradictory outcomes force to acquire a compromise between the best solution for the customer (highest economic benefits) and the government (highest energy and environmental savings). As it was commented in the previous section, the decision-making method searches for maximizing a global objective function, obtained

from an equal-weighted (EW) sum of both output indicators (ES and IRR, as single and independent objective functions), among all the possibilities. For this purpose, figure 10 shows how to proceed:

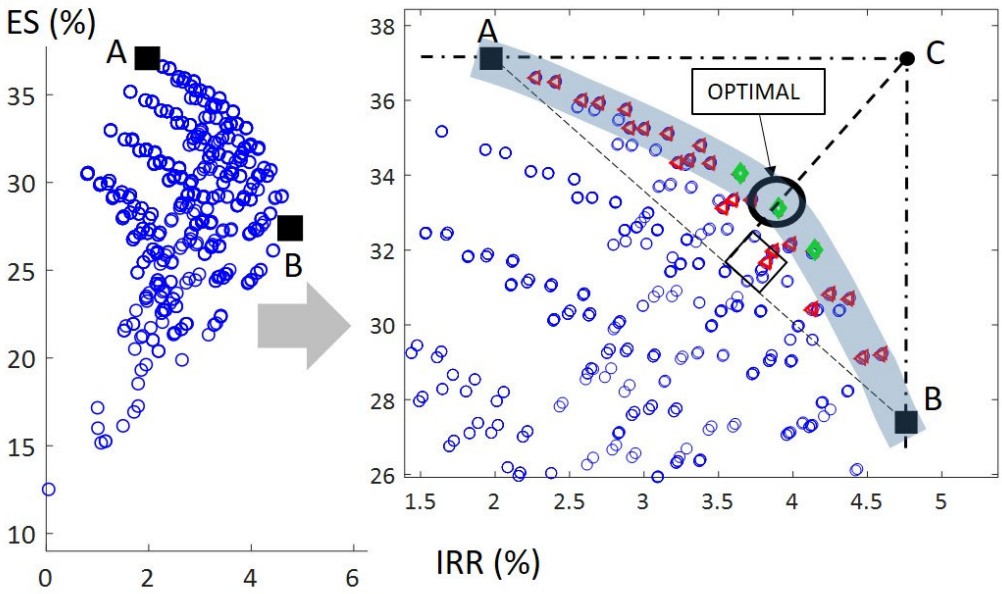

Figure 10. Pareto optimum solution from decision-making process.

i) A two-dimensional space represents all the results (cloud of dots) concerning ES and IRR for each case, where the ground loads are always balanced. The frontal curve (Pareto 2D front, gross line in figure 10) shows the frontier, which includes all the optimums related to one parameter, maintaining constant another one. It means that there are candidates to be selected as optimal for every case, although they present contradictory objectives. This behavior is directly related to the number and depth of the boreholes: a higher L_{GHE} supposes a more efficient heat transfer and successfully, energy savings, but the investment cost I_{GHE} increases, so the corresponding IRR becomes lower. The extreme cases

are the opposite: for a maximum ES (point A in figure 10), the IRR reaches a minimum value. On the contrary, the maximum IRR (point B in figure 10) supposes a minimum of ES.

ii) The equal-weighted Pareto's optimal solution finds a compromise between both objectives (the three nearest candidates have been marked with diamonds in figure 10, belonging to this front) in the following way: first, it traces a line that connects the extreme cases (A and B), and second, a perpendicular straight line is drawn to match with the so-called equilibrium point (point C in figure 10). The final conciliating design is located at the intersection point between the perpendicular and the Pareto's front. It coincides with this point with maximum curvature (elbow of the front, as it has been already suggested) [16]. Moreover, due to applying the same weight to both objectives, this perpendicular is bisector (with an angle of 45º) to the vertical and horizontal lines that, starting from A and B, match in C.

Among all the possible optimums, results marked with triangles (the major of them included in the Pareto's front) maintain the same decision values about $T_{f,U}$ (37.5ºC) and $N_{reg,R}$ (0h). As suggested previously, reducing the shave factor in the hybridization strategy provides better results than regenerating the soil. In addition, the most external cases in the front correspond to a rectangular distribution of the GHE. Allocating all the boreholes into a quite limited surface (540m^2) with this shape, makes the ground response more relaxed than with quincunx dissemination and prevents soil saturation more easily. Thus, lower temperatures of the fluid in summer (and higher in winter) are allowed.

Table 4 shows the main characteristics for the selected case, as well as for the bests single-optimal. The energetic finest (point A) presents the highest energy savings. However, it implies an important investment for an L_{GHE} greater than 3300 m, risking its economic availability, as its IRR is below the minimum recommended of 3.5%. On the contrary, the maximum IRR, which presents the B case with lower investment costs, provides an ES below 30%, far from other solutions to comply with decarbonization objectives satisfactorily. Moreover, the shave factor in all cases is the maximum possible in winter, while in summer, it is also maintained for the solutions at optimal and point A.

Table 4. GHE characteristics for the optimal solution.

Parameter/Case		Multi-objective optimized (equal-weighted)	Single-objective energetic optimal (point A, fig. 10)	Single-objective economic optimal (point B, fig. 10)
Inputs	Disposition	Rectangular	Rectangular	Rectangular
	N_b (number of boreholes)	18	24	18
	H (borehole deep, m)	120	140	80
	$T_{f,U}$ (ºC)	37.5	30	37.5
	$N_{reg,R}$ (daily nr. hours)	0	0	0
Outputs	L_{GHE} (m)	2160	3360	1440
	SF_{GHE} (%) Annual (winter – summer)	89.08 (91.2 – 86.6)	89.08 (91.2 – 86.6)	82.81 (91.2 – 72.94)
	ES (%)	33.12	37.11 (maximum)	27.4
	IRR (%)	3.9	1.97	4.76 (maximum)

From an energy point of view, the evaluated solutions are adapted to the hybridization strategies. Nevertheless, from an economic perspective, significant variations can occur due to two reasons: first, the electricity prices can significantly oscillate over time; and second, because of the promotion of the use of renewable energies, the facilities can receive financial aid from the government for their start-up. For these reasons, a sensitivity analysis has been included for the design point (optimal case). The IRR (%) variation has been evaluated, depending on the electricity price (taxes included) c_e (€/kWh) and investment grant IG (%), defined as a percentage of the investment costs of the final selected design.

892 Results can be observed in figure 11, where the selected solution without
893 changes has been marked with black dots, and dash-dot lines present the lower limit of
894 3.5% for IRR. Figure 11 depicts the economic benefits that this solution represents
895 nowadays, where instability of the electricity markets has increased the prices
896 significantly, as well as the advantage that may suppose the government aids to promote
897 this renewable source. Although the IRR obtained in this work is near the limit (3.5%),
898 the aim in these official buildings is mainly the energy savings, being profitability a less
899 critical parameter. Moreover, if the electricity price rises, the IRR will also increase
900 (figure 11.c). Changes in the economic scenarios may imply higher IRRs to make
901 decisions. For example, if the Spanish 10-year bond rises up to 2%, the reference IRR
902 can reach 5% (3%+2%), requiring higher electricity costs and government aid.
903

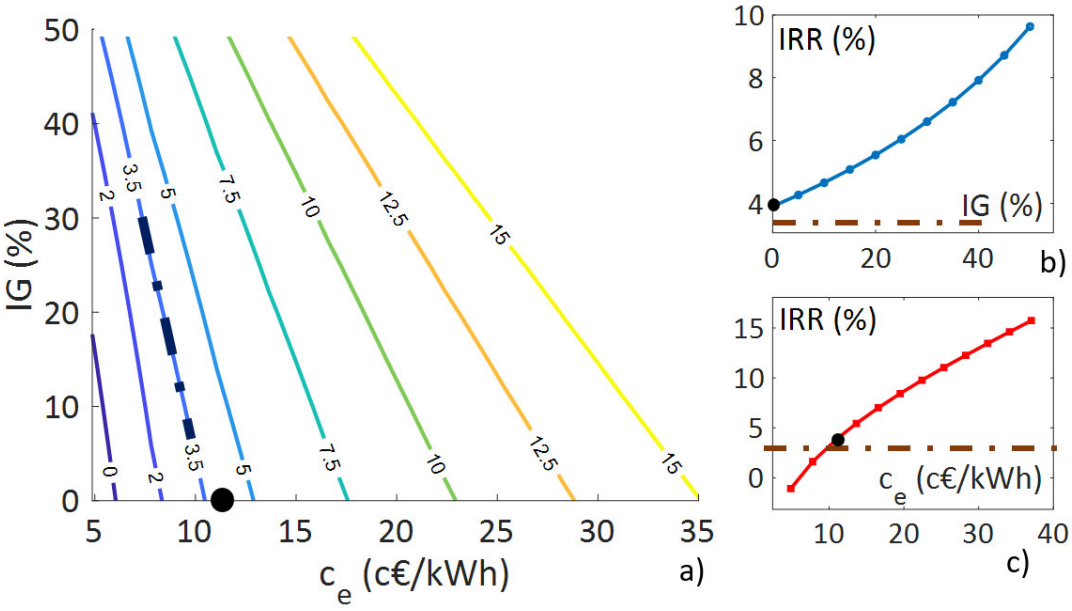

904

905 **Figure 11**. Sensitivity analysis of IRR for the final design: a) two-parameter sensitivity surface (from IG
906 and c_e); b) single-parameter *IG* sensitivity (constant c_e = 11.5c€/kWh); c) single-parameter c_e sensitivity
907 (constant IG = 0%).
908

909 Summarizing, the described DoE established a set of 896 cases for the different
910 combinations of input factors to be evaluated (varying number, depth, and disposition of
911 the GHE boreholes, as well as considering different possibilities about regeneration and
912 hybridization). The GSHP energy model that evaluates each of those cases provides a
913 highly realistic approach: i) the valuation of intermittent behaviour of GHEs, with
914 hourly aggregated loads, constitutes a quite precise modelling; ii) it is also favoured by
915 using an experimental based STGF, from which construct the global GHE g-function,
916 completing a more reliable ground characterization; iii) finally, the HP operation can be
917 satisfactorily replicated using the efficiency approach functions f_{COP} and f_{EER}, generated
918 from manufacturer available data. Among the possible optimal solutions (see Pareto's
919 front in figure 10), all of them comply with a rectangular disposition of boreholes and
920 develop better the hybridization strategy compared to using regeneration cycles (they
921 are not necessary here). Finally, the selected solution allows an ES and an IRR higher
922 than 33% and 3.9%, respectively. In addition, the sensitivity analysis applied to that
923 final solution demonstrates that scenarios with higher electricity prices and government
924 aid can increase its profitability significantly (see figure 11).
925
926 **4. Conclusions.**
927
928 The detailed energy model (with intermittent behavior of GHE, efficiencies
929 functions, and experimentally based STGF), together with regeneration and
930 hybridization strategies implemented in this study (see figure 4), allows reaching an
931 effective yearly balance of the ground thermal loads and operate the HP into its most
932 effectiveness range (see figure 7). It assures significant energy savings, CO_2 emissions
933 reductions, and no soil saturation for each simulated case concerning a given set of five

input factors (r/q, N_b, H, $T_{f,U}$ and $N_{reg,R}$). Furthermore, among all the possible solutions, the best set complies with a rectangular disposition of the GHE field and does not need regeneration cycles (see figure 11).

Pareto's optimally method has been used to find the best solution, searching for a compromise between both single-objectives, allowing an ES and an IRR higher than 33% and 3.9%, respectively. The sensitivity analysis applied to this solution (see figure 11) shows that scenarios with higher electricity prices and government aid can significantly increase its profitability.

This multi-objective optimization implies a not excessive number of simulations to be carried out (below 1000), even less than with other methods (both conventional and intelligent). It supposes a fast procedure for an optimal design of a GSHP, being quite friendly for the user.

Finally, future works should consider more combinations between different variables such as number, diameter, deep, U-tube, 2U-tube, and arrangement of boreholes and several HP devices.

ACKNOWLEDGMENTS.

This work has been supported by a research contract at the University of Jaen (Spain) (code 2406).

References.

1. Consejería de Agricultura, Ganadería, Pesca y Desarrollo Sostenible. Junta de Andalucía, 2022. Available at:

https://www.juntadeandalucia.es/medioambiente/portal/landing-page-%C3%ADndice/-/asset_publisher/zX2ouZa4r1Rf/content/climatolog-c3-ada-y-meteorolog-c3-ada-en-andaluc-c3-ada/20151

2. Ahmadi MH, Ahmadi MA, Sadaghiani MS, Ghazvini M, Shahriar S, Alhuyi Nazari M. Ground source heat pump carbon emissions and ground-source heat pump systems for heating and cooling of buildings: A review. Environ Prog Sustainable Energy. 2018;37:1241-65; doi: 10.1002/ep.12802.

3. Lund JW, Toth AN. Direct utilization of geothermal energy 2020 worldwide review. Geothermics. 2021;90:101915; doi: 10.1016/j.geothermics.2020.101915.

4. Eurostat, Statistics explained, 2022. Available at: https://ec.europa.eu/eurostat/statistics-explained/index.php?title=Renewable_energy_statistics#Over_one_fifth_of_energy_used_for_heating_and_cooling_from_renewable_sources

5. Arrizabalaga I, De Gregoria M, Garcia de la Noceda, C, Hidalgo R, Urchueguia JF. Country update for the Spanish geothermal sector. In Proceedings, World Geothermal Congress. 2015;19-24.

6. Jalaluddin, Miyara A. Thermal performance investigation of several types of vertical ground heat exchangers with different operation mode. Appl Therm Eng. 2012;33-34:167-74; doi: 10.1016/j.applthermaleng.2011.09.030.

7. Fadejev J, Simson R, Kurnitski J, Haghighat F. A review on energy piles design, sizing and modelling. Energy. 2017;122:390-407; doi: 10.1016/j.energy.2017.01.097.

8. Ahmadfard M, Bernier M. A review of vertical ground heat exchanger sizing tools including an inter-model comparison. Renewable Sustainable Energy Rev. 2019;110:247-65; doi: 10.1016/j.rser.2019.04.045.

9. Claesson J, Eskilson P. Conductive heat extraction to a deep borehole: Thermal analyses and dimensioning rules. Energy. 1988;13:509-27; doi: 10.1016/0360-5442(88)90005-9.

10. Eskilson P. Thermal analysis of heat extraction boreholes (Ph.D. thesis), Lund Inst. of Tech., Sweden, 1987.

11. Li M, Lai ACK. New temperature response functions (G functions) for pile and borehole ground heat exchangers based on composite-medium line-source theory. Energy. 2012;38:255-63; doi: 10.1016/j.energy.2011.12.004.

12. Diao NR, Zeng HY, Fang ZH. Improvement in modeling of heat transfer in vertical ground heat exchangers. HVAC R Res. 2004;10:459-70; doi: 10.1080/10789669.2004.10391114.

13. Yavuzturk C, Spitler JD. Short time step response factor model for vertical ground loop heat exchangers. ASHRAE Trans. 1999;105:PART 2/

1009 14. Pasquier P, Zarrella A, Labib R. Application of artificial neural networks to near-
1010 instant construction of short-term g-functions. Appl Therm Eng. 2018;143:910-21; doi:
1011 10.1016/j.applthermaleng.2018.07.137.
1012
1013 15. Cruz-Peragón F, Casanova-Peláez PJ, López-García R, Palomar-Carnicero JM.
1014 Extending capabilities of Thermal Response Tests in vertical ground heat exchangers:
1015 An experiment-based local short-time temperature response factor. Appl Therm Eng.
1016 2020;178:115606; doi: 10.1016/j.applthermaleng.2020.115606.
1017
1018 16. Aditya GR, Narsilio GA. Environmental assessment of hybrid ground source heat
1019 pump systems. Geothermics. 2020;87:101868; doi: 10.1016/j.geothermics.2020.101868.
1020
1021 17. Park H, Lee JS, Kim W, Kim Y. The cooling seasonal performance factor of a
1022 hybrid ground-source heat pump with parallel and serial configurations. Appl Energy.
1023 2013;102:877-84; doi: 10.1016/j.apenergy.2012.09.035.
1024
1025 18. Allaerts K, Coomans M, Salenbien R. Hybrid ground-source heat pump system with
1026 active air source regeneration. Energy Convers Manage. 2015;90:230-7; doi:
1027 10.1016/j.enconman.2014.11.009.
1028
1029 19. Liu Z, Xu W, Zhai X, Qian C, Chen X. Feasibility and performance study of the
1030 hybrid ground-source heat pump system for one office building in Chinese heating
1031 dominated areas. Renew Energy. 2017;101:1131-40; doi: 10.1016/j.renene.2016.10.006.
1032

1033 20. Yavuzturk C, Spitler JD. Comparative study of operating and control strategies for
1034 hybrid ground-source heat pump systems using a short time step simulation model.
1035 ASHRAE Trans. 2000;106:PA/
1036
1037 21. Sanner B, Hellström G, Spitler J, Gehlin S. Thermal response test–current status and
1038 world-wide application. In Proceedings world geothermal congress. 2005;1436.
1039
1040 22. Casanova-Peláez PJ, Palomar-Carnicero JM, López-García R, Cruz-Peragón F.
1041 Development of device for ground thermal response tests (TRT) in geothermal
1042 installations. Dyna (Spain) 2014;89(3):316-24.
1043
1044 23. Bejan A, Tsatsaronis G, Moran MJ. Thermal design and optimization. : John Wiley
1045 & Sons; 1995.
1046
1047 24. Investing.com, 2022. Available at: https://es.investing.com/rates-bonds/spain-10-
1048 year-bond-yield-historical-data
1049
1050 25. Eur-lex. Directive (EU) 2018/2002 of the European Parliament and of the Council
1051 of 11 December 2018 amending Directive 2012/27/EU on energy efficiency, 2018.
1052 Available at: https://eur-lex.europa.eu/legal-
1053 content/EN/TXT/?uri=uriserv%3AOJ.L_.2018.328.01.0210.01.ENG
1054
1055 26. BOE. Ley 24/2013 de 26 de diciembre, del Sector Eléctrico, 2013. Available at:
1056 https://www.boe.es/buscar/doc.php?id=BOE-A-2013-13645
1057

1058 27. Van Veldhuizen DA, Lamont GB. Multiobjective evolutionary algorithms:
1059 analyzing the state-of-the-art. Evol Comput. 2000;8:125-47; doi:
1060 10.1162/106365600568158.
1061
1062 28. Gill PE, Murray W, Wright MH. Practical optimization. SIAM; 2019.
1063
1064 29. Pham D, Karaboga D. Intelligent optimisation techniques: genetic algorithms, tabu
1065 search, simulated annealing and neural networks. : Springer Science & Business Media;
1066 2012.
1067
1068 30. Bozzoli F, Pagliarini G, Rainieri S, Schiavi L. Estimation of soil and grout thermal
1069 properties through a TSPEP (two-step parameter estimation procedure) applied to TRT
1070 (thermal response test) data. Energy. 2011;36:839-46; doi:
1071 10.1016/j.energy.2010.12.031.
1072
1073 31. Li M, Lai ACK. Parameter estimation of in-situ thermal response tests for borehole
1074 ground heat exchangers. Int J Heat Mass Transf. 2012;55:2615-24; doi:
1075 10.1016/j.ijheatmasstransfer.2011.12.033.
1076
1077 32. Sayyaadi H, Amlashi EH, Amidpour M. Multi-objective optimization of a vertical
1078 ground source heat pump using evolutionary algorithm. Energy Convers Manage.
1079 2009;50:2035-46; doi: 10.1016/j.enconman.2009.04.006.
1080
1081 33. Bianco N, Fragnito A, Iasiello M, Maria Mauro G. A comprehensive approach for
1082 the multi-objective optimization of Heat Recovery Steam Generators to maximize cost-

1083 effectiveness and output power. Sustainable Energy Technol Assess. 2021;45; doi:
1084 10.1016/j.seta.2021.101162.
1085
1086 34. Hu S, Li J, Yang F, Yang Z, Duan Y. Multi-objective optimization of organic
1087 Rankine cycle using hydrofluorolefins (HFOs) based on different target preferences.
1088 Energy. 2020;203; doi: 10.1016/j.energy.2020.117848.
1089
1090 35. Park K, Ahn J-. Design of experiment considering two-way interactions and its
1091 application to injection molding processes with numerical analysis. J Mater Process
1092 Technol. 2004;146:221-7; doi: 10.1016/j.jmatprotec.2003.10.020.
1093
1094 36. Park H, Kim W, Lee JS, Kim Y. Optimization of a hybrid ground source heat pump
1095 using the response surface method. In World Renewable Energy Congress-Sweden
1096 2011:1345-51.
1097
1098 37. Khalajzadeh V, Heidarinejad G, Srebric J. Parameters optimization of a vertical
1099 ground heat exchanger based on response surface methodology. Energy Build.
1100 2011;43:1288-94; doi: 10.1016/j.enbuild.2011.01.007.
1101
1102 38. Pu L, Qi D, Xu L, Li Y. Optimization on the performance of ground heat
1103 exchangers for GSHP using Kriging model based on MOGA. Appl Therm Eng.
1104 2017;118:480-9; doi: 10.1016/j.applthermaleng.2017.02.114.
1105

39. Cullin JR, Spitler JD, Montagud C, Ruiz-Calvo F, Rees SJ, Naicker SS, Konečný P, Southard LE. Validation of vertical ground heat exchanger design methodologies. Sc Tech Built Environ. 2015;21:137-49; doi: 10.1080/10789669.2014.974478.

40. Ministerio para la Transición Ecológica y el Reto Demográfico. HULC software, 2021. Available at: https://energia.gob.es/desarrollo/EficienciaEnergetica/CertificacionEnergetica/DocumentosReconocidos/Paginas/procedimientos-certificacion-proyecto-terminados.aspx.

41. Lawrence Berkeley National Laboratory. DOE-2.2, 2021. Available at: https://www.energy.gov/ea/lawrence-berkeley-national-laboratory. DOE-2.2.

42. Pagliarini G, Rainieri S. Restoration of the building hourly space heating and cooling loads from the monthly energy consumption. Energy Build. 2012;49:348-55.

43. Choi JC, Lee SR, Lee DS. Numerical simulation of vertical ground heat exchangers: Intermittent operation in unsaturated soil conditions. Comput Geotech. 2011;38:949-58.

44. Gehlin S, Nordell B. Determining undisturbed ground temperature for thermal response test. ASHRAE Transactions. 2003;109 PART 1:151-6.

45. Witte HJL, Van Gelder GJ, Spitler JD. In situ measurement of ground thermal conductivity: A dutch perspective. ASHRAE Trans. 2002;108 PART 1:263-72

46. Zeng H, Diao N, Fang Z. Heat transfer analysis of boreholes in vertical ground heat exchangers. Int J Heat Mass Transfer. 2003;46:4467-81.

47. Yavuzturk C, Spitler JD, Rees SJ. A Transient two-dimensional finite volume model for the simulation of vertical U-tube ground heat exchangers. ASHRAE Trans. 1999;105:PART 2/

48. Red Eléctrica de España. Available at: https://www.ree.es/es

49. Wu CFJ, Hamada M. Experiments: planings, analysis and parameter design optimization. New Jersey, EEUU: John Wiley & Sons; 2009.

50. Weissman SA, Anderson NG. Design of Experiments (DoE) and Process Optimization. A Review of Recent Publications. Org Process Res Dev. 2015;19:1605-33; doi: 10.1021/op500169m.

51. Cruz-Peragón F, Jiménez-Espadafor FJ. A genetic algorithm for determining cylinder pressure in internal combustion engines. Energy Fuels. 2007;21:2600-7; doi: 10.1021/ef0605495.